

A study of pre-equilibrium emission in some proton induced reactions: Measurement of cross-sections

B. P. Singh¹, M.M. Musthafa², H.D.Bhardwaj³, Devendra P. Singh¹, Pushpendra P. Singh¹,
Abhishek Yadav¹, Unnati¹, Manoj K. Sharma¹, and R.Prasad¹

¹Department of Physics A. M. University, Aligarh 202002 (U.P.), India

²Department of Physics, Calicut University, Calicut, India

³Department of Physics, DSN College, Unnao, India

Email contact of main author: bpsinghamu@gmail.com

Abstract. In the present work excitation functions (EFs) for several proton-induced reactions up to ≈ 20 MeV have been measured using the proton beam from Variable Energy Cyclotron Centre, Kolkata, INDIA. The stacked foil activation technique followed by off-line gamma-ray spectroscopy has been employed. The theoretical calculations have been carried out using the semi-classical model code, ACT which includes both compound nucleus (CN) as well as pre-equilibrium (PE) emission. Analysis of data suggests that pre-equilibrium emission reaction mechanism is important at these energies and should be included in theoretical calculations to reproduce the experimental data. The pre-equilibrium emission is found to be dominant at relatively higher energies.

1. Introduction

The study of nuclear reactions induced by protons has again attracted the attention of nuclear physicists. One of the main reasons for this is the requirement of precise nuclear data needed for the development of recently proposed Accelerator Driven Sub-critical (ADS) reactors [1]. Further, the data also have verity of applications including the field of medical sciences, environmental sciences, transmutation of nuclear waste etc. One of the important aim of the study of such reactions is to enhance the basic understanding of the reaction mechanism. The reaction mechanism of nucleon induced reactions particularly proton induced reactions is still not well understood. There are indications that compound and pre-compound reaction processes play an important role at moderate excitation energies [6-14]. The nuclear data for the accelerator driven technologies are required for a large number of the target elements covering almost entire periodic table over a wide range of energies. As such, more detailed and accurate measurements are needed to fulfill this requirement of data. The nuclear data required for these applications are obtained mainly from the nuclear scattering and from the reaction model calculations, which depend on the optical models, whose parameters are determined by elastic scattering and the total cross-section data. Efforts have been made to obtain the estimates of basic nuclear reaction cross-sections both experimentally as well as theoretically. Though, considerable data is available in literature on nucleon induced reactions but the cross-section values measured by different groups of workers for the same reaction, generally, do not agree. Further, earlier measurements were done mostly by using detectors and electronics of low resolution and poor efficiency. As such, it has been realized that there is a great need of new, reliable and self consistent cross-section data taken by high resolution detectors of better efficiency. It may not be out of place to mention that theoretically it may be possible to explain the measured excitation function (EFs) for a given reaction channel individually using a certain theoretical code. However, a consistent analysis requires reproduction of excitation function for all open channels simultaneous using the same code. Fitting of excitation function for an individual channel may improve the description of the data for the partial channel at the cost of other open channels however, it is unacceptable from

the point of view of physics. Several phenomenological as well as quantum-mechanical models have been launched to explain the pre-equilibrium (PE) reaction mechanism. All these models describe the method by in which projectile energy gradually gets redistributed among the constituent nucleons of the composite system through a series of residual two-body interactions. It is interesting to obtain in the analysis, simultaneously, a best description of all existing experimental data for all open channels, as this approach is considered to be internally consistent, detailed and complete. Several models like ALICE-91 [2, 3], CASCADE [4], PACE2 [5], ACT [6], COMPLETE [7] etc., are available in the literature and are generally used for theoretical calculations of EFs for light and heavy-ion induced reactions. In all the codes except ACT [6], the configuration of the codes is such that they predict the total cross-section only for the population of the residual nuclei. However, the code ACT [6] calculates the cross-sections for the production of both the ground as well as isomeric states. In the present work, the code ACT [6] based on the lines of codes STAPRE [8] has been used in the present work using consistently the same set of parameters. At moderate excitation energies, reactions induced by nucleons and light-heavy ions are found to proceed through CN as well as PE emission [9]. As such, precise measurement of EFs for such cases and their analysis may be used to find out the relative contribution of equilibrium and PE processes. With a view to provide a large set of cross-section data and to study the mechanism of PE emission, a programme of precise measurement and analysis of cross-sections for proton, alpha-particles and heavy-ion induced reactions [9-14] has been undertaken. These measurements may provide a broad database for testing the capability of theoretical model codes with respect to calculating ratio-isotope production. The experimental details are given in section 2, while the details of result and discussion are given in section 3 of the paper.

2. Experimental Details

The present experiments have been carried out at the Variable Energy Cyclotron Centre (VECC), Kolkata, India, using a collimated proton beam of $\approx 20\text{MeV}$. Self-supporting spectroscopically pure foils of different materials have been used as targets. The thickness of the commercially supplied foils was $\approx 2\text{mg/cm}^2$. The target stacks containing several samples having aluminum degraders in between them were bombarded separately by proton beams in the irradiation chamber dedicated to this purpose for times ranging from half an hour to several hours depending on the half life of interest. A beam current $\approx 100\text{ nA}$ was used and was monitored from current integrator count rate. The average beam energy on a given target foil and/or degrader was calculated using the stopping-power values given in the tables of Northcliffe and Schilling [15]. A typical stack arrangement used for irradiation of the targets is shown in Fig.1.

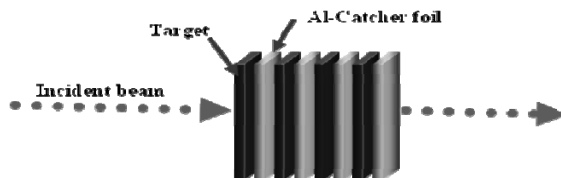


Figure 1. Stack arrangement for the measurement of excitation functions.

The main advantage of this technique is that as the beam traverses the samples in the stack, it loses its energy and hence the different samples of the stack are bombarded at different energies. As such, in a single irradiation several foils are bombarded at different energies and hence reducing the beam time requirement. Post-irradiation analysis has been performed using

a high-resolution HPGe detector coupled to a multichannel analyzer. The HPGe detector, was pre-calibrated for energy as well as efficiency, using various standard γ -sources. A ^{152}Eu point source was also used to determine the efficiency of the detector for different γ -ray energies at several source detector distances. The sample and detector distances were suitably adjusted so as to minimize the dead time $< 10\%$. The decay data [16] used in the present work for yield calculations are given in Table 1. The residues produced due to different reaction channels were identified by their characteristic γ -rays and measured half-lives. From the observed activities of the residual nuclei, the cross-sections for a given reaction channel were determined using the standard formulation as given below [17]:

$$\sigma_r(E) = A\lambda \exp(\lambda t_2) / \{N_0 \phi \theta K(G_\epsilon) [1 - \exp(-\lambda t_1)] [1 - \exp(-\lambda t_3)]\} \dots\dots\dots(1)$$

where, A is the observed counts (area under the photo peak of the characteristic gamma ray of the particular residues) during the accumulation time t_3 of the induced activity of the decay constant λ , N_0 the number of target nuclei being exposed under the geometrical shadow of the beam irradiated for duration t_1 with a particle beam of flux ϕ , t_2 the time lapse between the stop of irradiation and the start of counting, μ the branching ratio of the characteristic γ -ray and G_ϵ the geometry-dependent efficiency of the detector. The factor $[1 - \exp(-\lambda t_1)]$ takes care of the decay of evaporation residue during the irradiation and is typically known as the saturation correction. The correction for the decay of the induced activity due to the delay between the stop of irradiation and the start of counting and during the data accumulation is taken into account via the factors $\exp(\lambda t_2)$ and $[1 - \exp(-\lambda t_3)]$, respectively. $K = [1 - \exp(-\mu d)] / \mu d$ is the correction for the self-absorption of the γ -radiation in the sample thickness itself, where d is the thickness of the sample and μ is the γ -ray absorption coefficient. Often the same residual nucleus decay by emitting several gamma rays of different energies having different branching ratios. In such cases, cross-section for the same channel has been determined from the measured intensity of each detected gamma ray. The result quoted is the weighted average of each individual cross-section value [18].

Several factors may introduce uncertainties in the present measurements and are discussed here. There may be uncertainty in determining the geometry-dependent detector efficiency. The statistical errors of the counting of the standard sources may also give rise to the error in efficiency, which was minimized by accumulating large number of the counts for comparatively larger times (≈ 5000 s). The uncertainty due to fitting of the efficiency curve is estimated to be $< 3\%$. Uncertainty in determining the efficiency may also come up due to the solid-angle effect, because the irradiated samples were not point sources like the standard source, but they had a diameter of $\approx 3\text{mm}$. Correction for this has been applied as given in ref.[19]. The inaccurate estimate of the foil thickness and non-uniformity of foil may give rise to uncertainty in determining the number of target nuclei in the sample. It is estimated from the thickness measurements at different positions of the sample foils that errors due to non-uniform deposition are expected to be $< 1\%$. Errors may come up due to fluctuations in beam current during the irradiation. It is estimated that beam fluctuations may introduce error of $< 3\%$. During irradiation of the stack, the beam traverses the thickness of the material, thus the initial beam intensity gets reduced. It is estimated that the error due to decrease in beam intensity is expected to be $< 2\%$. In all these measurements the dead time is kept less than 10% by suitably adjusting the sample-detector distance and the corrections for it were applied in the counting rates. Further, the uncertainties in the branching ratio, decay constant, half-lives etc., which are taken from the table of isotopes have not been taken into account. The overall error due to all these factors is expected to be $< 15\%$ of the measured cross-section values.

3. Results and Discussion

The EFs for various reactions in several target nuclei viz., ^{51}V , ^{58}Ni , ^{60}Ni , ^{61}Ni , ^{62}Ni , ^{63}Cu , ^{65}Cu , ^{89}Y , ^{93}Nb , ^{119}In , ^{121}Sb , ^{123}Sb , ^{130}Te , and ^{197}Au using proton and alpha beam have been measured. Excitation functions for the reactions $^{60}\text{Ni}(p,n)$, $^{61}\text{Ni}(p,n)$, $^{93}\text{Nb}(p,n)$, $^{121}\text{Sb}(p,n)$, $^{123}\text{Sb}(p,n)$ and $^{130}\text{Te}(p,n)$ have already been published [12]. In the present work EFs for the reactions $^{63}\text{Cu}(p,n)$, $^{63}\text{Cu}(p,2n)$, $^{65}\text{Cu}(p,n)$, $^{197}\text{Au}(p,n)$, $^{197}\text{Au}(p,np)$, $^{89}\text{Y}(p,n)$, $^{93}\text{Nb}(p,n)$, $^{123}\text{Sb}(p,np)$ and $^{58}\text{Ni}(p,\alpha)$ are reported. The spectroscopic data for these reactions are presented in Table I.

TABLE: 1 MEASURED REACTION CHANNELS WITH THEIR SPECTROSCOPIC PROPERTIES

S.No	Reaction	Residue	Half-life($T_{1/2}$)	$E_\gamma(\text{keV})$	B. R. (%)
1.	$^{63}\text{Cu}(p,n)$	^{63}Zn	38.1 min	669.8, 926.2	8.4, 6.6
2.	$^{63}\text{Cu}(p,2n)$	^{62}Zn	9.3h	548.4, 596.7	15.2, 25.7
3.	$^{65}\text{Cu}(p,n)$	^{65}Zn	244.1d	1115.5	50.7
4.	$^{197}\text{Au}(p,n)$	^{197g}Hg	2.7d	80.4	3.3
5.	$^{197}\text{Au}(p,n)$	^{197m}Hg	23.8h	134.0	47.2
6.	$^{197}\text{Au}(p,np)$	^{196m}Au	9.7h	147.8, 188.2	47.2, 34.4
7.	$^{89}\text{Y}(p,n)$	^{89g}Zr	3.3d	909.1	99.0
8.	$^{89}\text{Y}(p,n)$	^{89m}Zr	4.2 min	587.7	89.5
9.	$^{123}\text{Sb}(p,np)$	^{122}Sb	2.7d	564.37	70.0
10.	$^{93}\text{Nb}(p,n)$	^{93m}Mo	6.8h	263.1, 684.8	56.7, 99.7
11.	$^{58}\text{Ni}(p,\alpha)$	^{55}Co	17.5h	477.2, 931.2	20.2, 75.0

The experimentally measured cross-sections for reactions $^{63}\text{Cu}(p,n)^{63}\text{Zn}$, $^{63}\text{Cu}(p,2n)^{62}\text{Zn}$ and $^{65}\text{Cu}(p,n)^{65}\text{Zn}$ reported upto 20 MeV are given in Table 2. The residue ^{63}Zn decays via 38.1 min half-life by emitting γ -rays of ≈ 669 keV and ≈ 926 keV, while the residues ^{62}Zn and ^{65}Zn decay with 9.3h and 244 days half-lives by emitting gamma-rays of energy ≈ 548 & 596 keV and 1115 keV, respectively. Since, the Q-value of the reaction $^{63}\text{Cu}(p,2n)^{62}\text{Zn}$ is ≈ 15 MeV, as such below this energy there is no data shown in Table 2.

TABLE 2: THE EXPERIMENTALLY MEASURED CROSS-SECTIONS FOR THE REACTIONS $^{63}\text{Cu}(p,n)$, $^{63}\text{Cu}(p,2n)$ AND $^{65}\text{Cu}(p,n)$

Energy (MeV)	Cross-section (mb)		
	$^{63}\text{Cu}(p,n)^{63}\text{Zn}$	$^{63}\text{Cu}(p,2n)^{62}\text{Zn}$	$^{65}\text{Cu}(p,n)^{65}\text{Zn}$
06.68 \pm 0.54	57.25 \pm 7.8	----	278.63 \pm 36.1
09.00 \pm 0.53	385.42 \pm 50.1	----	515.36 \pm 66.9
11.53 \pm 0.53	565.26 \pm 73.6	----	652.69 \pm 85.6
13.74 \pm 0.52	437.32 \pm 56.8	----	474.37 \pm 88.9
16.06 \pm 0.52	279.28 \pm 44.8	20.70 \pm 3.3	256.52 \pm 35.9
18.00 \pm 0.52	89.31 \pm 11.7	45.30 \pm 6.3	93.32 \pm 15.4
20.00 \pm 0.51	63.20 \pm 8.9	98.32 \pm 12.7	47.15 \pm 7.2

The reactions $^{123}\text{Sb}(p,np)$, $^{93}\text{Nb}(p,n)$ and $^{58}\text{Ni}(p,\alpha)$ produce $^{122}\text{Sb}(t_{1/2} = 2.7\text{d}, E_{\gamma} = 564.3\text{ keV})$, $^{93\text{m}}\text{Mo}(t_{1/2} = 6.8\text{h}, E_{\gamma} = 263.1\text{ keV and } 684.8\text{ keV})$ and $^{55}\text{Co}(t_{1/2} = 17.5\text{h}, E_{\gamma} = 477.2\text{ keV and } 931.2\text{ keV})$. The measured cross-sections for these reaction channels are given in TABLES: 3-5, respectively.

TABLE 3: THE EXPERIMENTALLY MEASURED CROSS-SECTIONS FOR THE REACTION $^{123}\text{Sb}(p,np)^{122}\text{Sb}$

Energy (MeV)	Cross-section (mb)
12.53±0.52	4.31±0.5
14.56±0.51	16.07±2.2
16.21±0.51	19.91±2.6
18.16±0.51	24.30±2.9
20.00±0.50	36.32±4.5

TABLE 4: THE EXPERIMENTALLY MEASURED CROSS-SECTIONS FOR THE REACTION $^{93}\text{Nb}(p,n)^{93\text{m}}\text{Mo}$ and $^{58}\text{Ni}(p,\alpha)^{55}\text{Co}$

Energy (MeV)	Cross-section (mb)	Energy (MeV)	Cross-section (mb)
05.41±0.70	5.83±0.70	07.08±0.56	----
06.81±0.67	17.26±2.5	09.00±0.56	17.50±2.6
08.76±0.65	28.26±3.8	10.00±0.55	18.02±2.7
10.39±0.63	42.68±5.5	12.10±0.55	30.30±3.2
11.15±0.62	59.31±9.3	13.50±0.54	22.30±3.9
12.00±0.61	85.62±11.5	15.00±0.54	23.32±3.9

The reaction $^{197}\text{Au}(p,n)$ produces both ground and meta stable states of ^{197}Hg which have 2.7d and 23.8h half-lives and decay by emitting 80 keV and 134 keV γ -rays, respectively. In Table: 6, the cross-sections for both the ground and meta-stable states of ^{197}Hg are given. Further, production cross-section for the isotope $^{196\text{m}}\text{Au}$, produced via reaction $^{197}\text{Au}(p,np)$ is also given in this Table 6. In the present work, only meta-stable state of ^{196}Au could be observed, which decays by 9.7 h half-life. Further, in case of $^{89}\text{Y}(p,n)$ reaction, the ground as well as meta-stable states of isotopes $^{89\text{g}}\text{Zr}$ and $^{89\text{m}}\text{Zr}$ of 3.3d and 4.2 min. half-lives, respectively have been observed. The ground and meta-stable states were identified by their characteristic γ -lines of 909 and 587 keV. The experimentally measured EFs for both meta-stable and ground states of Zr isotopes are given in Table 7. Further, in order to obtain the total cross-section of this neutron channel, the contribution of ground and meta-stable states is added.

TABLE 6: THE EXPERIMENTALLY MEASURED CROSS-SECTIONS FOR THE REACTIONS $^{197}\text{Au}(p,n)^{197\text{g}}\text{Hg}$, $^{197}\text{Au}(p,n)^{197\text{m}}\text{Hg}$ AND $^{197}\text{Au}(p,np)^{196}\text{Au}$

Energy (MeV)	Cross-section (mb)			
	$^{197}\text{Au}(p,n)^{197\text{g}}\text{Hg}$	$^{197}\text{Au}(p,n)^{197\text{m}}\text{Hg}$	$^{197}\text{Au}(p,n)^{197}\text{Hg}$	$^{197}\text{Au}(p,np)^{196}\text{Au}$
08.43±0.53	7.49±1.4	30.98±4.88	38.47±6.28	----
10.13±0.52	63.38±8.9	187.78±24.4	251.16±33.3	----
12.30±0.52	65.72±9.1	124.1±16.12	189.82±25.22	----
14.17±0.51	41.18±5.9	43.58±6.1	84.76±12.0	3.26±0.4
16.27±0.51	40.26±5.6	42.26±5.9	82.52±11.5	21.84±3.5

18.15±0.51	28.69±4.2	29.27±3.7	57.96±7.9	58.94±7.9
20.00±0.50	27.94±4.1	21.0±3.1	48.94±7.2	99.74±14.8

TABLE 7: THE EXPERIMENTALLY MEASURED CROSS-SECTIONS FOR THE REACTIONS $^{89}\text{Y}(p,n)^{89g}\text{Zr}$ AND $^{89}\text{Y}(p,n)^{89m}\text{Zr}$

Energy (MeV)	Cross-section (mb)		
	$^{89}\text{Y}(p,n)^{89g}\text{Zr}$	$^{89}\text{Y}(p,n)^{89m}\text{Zr}$	$^{89}\text{Y}(p,n)^{89g}\text{Zr}$
05.24±0.55	72.63±10.1	----	72.63±10.1
6.50±0.55	173.42±22.6	65.36±8.7	238.78±31.3
7.48±0.54	217.26±28.2	119.69±15.6	336.95±43.8
8.10±0.56	294.32±40.2	144.37±18.8	401.32±59.0
9.17±0.56	322.28±43.9	159.36±20.7	445.28±64.6
10.25±0.56	320.31±42.8	136.74±19.4	457.05±62.2
11.62±0.55	326.21±43.2	98.63±11.8	424.84±55.0
13.28±0.57	323.74±44.6	89.63±11.9	413.37±56.5
15.02±0.56	177.63±23.1	57.34±7.5	234.97±30.6

Several theoretical model based computer codes are available in literature to calculate the reaction cross-sections. In the present work, the analysis of the data has been done using the code ACT [6], which is based on the lines of code STAPRE [8]. In code ACT the Hauser-Feshbach (HF) theory [18] is used for CN calculations, while PE emission is simulated using exciton model [20]. In HF model the conservation of angular momentum is taken into account at each step of de-excitation. Further, in code ACT it is possible to calculate separately the production cross-sections for both ground as well as meta-stable states.

In code ACT, the level density parameter ‘ a ’, initial exciton number n_o , and the strength parameter F_M of the square of two-body residual interaction matrix element are some of the important parameters. The level density parameters ‘ a ’ are taken consistently from the tables of Dilg et. al., [21]. In the exciton model the intermediate states of the system are characterized by the excitation energy E and the number n_p of the excited particles and n_h of the holes. Initial configuration of the compound system defined by its exciton number $n_o(=n_p+n_h)$ is an important parameter of the PE formalism.

It is, therefore, important to find the initial exciton number and the assumed division of excitons into particles and holes required to reproduce the experimental data. In literature, values of $n_o=1-3$ are used for proton induced reactions. In the present analysis, choice of $n_o=3$ for proton induced reactions is found to give satisfactory reproduction of the experimental data. The value of $n_o=3$ for proton induced reactions, may be justified assuming that the first projectile-target interaction may give rise to the excitation of one particle above the Fermi energy leaving behind a hole in excited state i.e., in all $3(2p+1h)$ initial exciton states for proton induced reactions. It may be pointed out that a lower value of exciton number gives, in general, higher pre-equilibrium contribution. This is because a smaller value of exciton number means larger number of two-body interactions prior to the establishment of equilibration characteristic of the compound nucleus resulting in the large pre-equilibrium contribution. In order to calculate the internal transition rates it is necessary to calculate the value of matrix element $|M|$ for two-body residual interaction. However, in the absence of any microscopic calculations for $|M|$, the expression $|M|^2=F_M A^{-3} U^{-1}$ (where, A and U are the mass

number and excitation energy of the compound system respectively) given by Kalbach-Cline [22] has, generally, been used, which relates the square of the average value of the matrix element by a strength parameter F_M of two-body residual interactions. The F_M may be treated as an adjustable parameter. Further, a lower value of F_M means a smaller value of $|M|^2$ and hence lower transition rates. As a result continuum decay rates for a given value of initial exciton number will relatively increase the pre-compound contribution. In literature, values of F_M having large variations have been used [23]. As a typical example the measured and calculated excitation functions for the reactions $^{93}\text{Nb}(p,n)^m$ and $^{63}\text{Cu}(p,2n)$ are shown along with the literature data in Fig. 2(a) & (b) respectively.

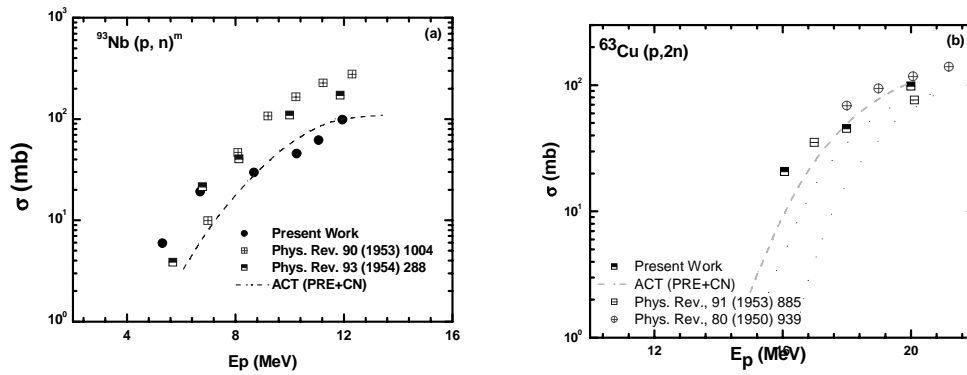


Fig 2(a-b): Experimentally measured and theoretically calculated EFs.

As can be seen from these figures and also from our earlier analysis of (p,n) reaction for a large number of reactions that, in the present calculations a value of $F_M=430\text{MeV}^3$ has been found to give satisfactory reproduction of almost all the data. In order to show the fitting of the data with calculations, as a typical example the experimentally measured and theoretically calculated excitation function for the reaction $^{130}\text{Te}(p,n)^{130}\text{I}$, which covers the tail portion [12] of the EF is shown in Fig.3. As such, calculations have been done by using consistent set of parameters. As can be seen from Fig. 3, that the high energy tail portion of EF is reproduced by same set of parameters giving confidence in our choice of parameters.

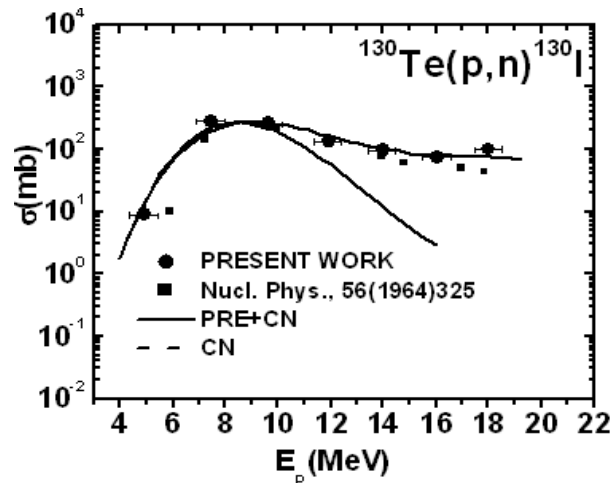


Fig.3 Experimentally measured and theoretically calculated EFs for $^{130}\text{Te}(p,n)^{130}\text{I}$ reaction.

In conclusions, it may be mentioned that, cross-sections for a large number of proton induced reactions have been measured from threshold to ≈ 20 MeV. Since, the high energy tail portion of the EFs could be reproduced by including PE component, as such, it may be concluded that PE emission plays a dominant role at relatively higher energies. An attempt has been made to fix the important parameters of the code ACT. The PE-component is found to be energy dependent.

4. Acknowledgements

The authors thank the VECC personnel for all their help and cooperation during the experiments. Authors are also thankful to the Chairman, Department of Physics, AMU for providing necessary facilities to carry out this work. Authors (MKS) thanks to DST, RPM to DST & UGC and AY to UGC-CSIR for providing financial support.

References

- [1] C. Rubbia et. al., Conceptual Design of a Fast Neutron Operated High Power Energy Amplifier, Report CERN/AT/95-94(ET).
- [2] M. Blann, Ann. Rev. Nucl. Sci. 25 (1975) 123.
- [3] M. Blann, NEA Data Bank, Gif-sur-Yvette, France, Report NO. PSR- (1991) 146.
- [4] F. Puhlhofer, Nucl. Phys. A280 (1977) 267.
- [5] A. Garvon, Phys. Rev. C 21, 230 (1980).
- [6] H.D. Bhardwaj, PhD Thesis, A.M.U. Aligarh, India (1985).
- [7] J. Ernst, W. Friedland, H. Stockhorst, Z. Phys. A 328, 333 (1987).
- [8] M. Uhl and B. Stromaier, Report IRK 76/01 (1981) NEA Data Bank (Cedex) France.
- [9] B.P. Singh, Ph.D. Thesis, AMU, Aligarh, India (1991).
- [10] M.M. Musthafa, Ph.D. Thesis, AMU, Aligarh, India (1996).
- [11] M.M. Musthafa, Manoj Kumar Sharma, B.P. Singh, R. Prasad, Applied Radiation and Isotopes 62 (2005) 419.
- [12] B.P. Singh, Manoj K. Sharma, M.M. Muthafa, H.D. Bhardwaj, R. Prasad, Nucl. Instrum. Methods Phys. Res. A 562, 717 (2006).
- [13] B.P. Singh, M.G.V. Sankracharyulu, M. Afzal Ansari, H.D. Bhardwaj, R. Prasad, Phys. Rev. C47 (1993) 2055.
- [14] M. M. Muthafa, B.P. Singh, M.G.V. Sankaracharyulu, H.D. Bhardwaj and R. Prasad, Phy. Rev. C52 (1995) 3174.
- [15] L.C. North Cliffe and R.F. Schilling, Nucl. Data Tables A7 (1970) 256.
- [16] C.M. Lederer, V.S. Shirley, Table of Isotopes VII (John Wiley, New York, 1978).
- [17] N.L. Singh et al., Can. J. Phys. 67, 870 (1989).
- [18] W. Hauser and H. Feshbach, Phys. Rev. 87 (1952) 366.
- [19] R.P. Gardner and K Verghese, Nucl. Inst. And Methods 93(1971)163.
- [20] J.J. Griffin, Phys. Rev. Lett. 17 (1966) 478.
- [21] W. Dilg, W. Schantl and H.K. Vonach, Nucl. Phys. A217 (1973) 269.
- [22] C.Kalbach-Cline, Nucl. Phys. A210 (1973) 590
- [23] K.K. Gudima, S.G. Mashnik and V.D. Toneev, Nucl. Phys. A401 (1983) 329.